Quaternary Cross-Diffusion in Water-in-Oil Microemulsions Loaded with a Component of the Belousov−Zhabotinsky Reaction

Federico Rossi,[†,‡] Vladimir K. Vanag,[†] Enzo Tiezzi,[‡] and Irving R. Epstein*[,†]

Department of Chemistry and Volen Center for Complex System, MS 015, Brandeis University, Waltham, 02454-9110, and Department of Chemistry, University of Siena, Siena, 53100 Italy

Received: March 26, 2010; Revised Manuscript Received: May 7, 2010

We obtain the diffusion matrix, **D**, consisting of the main and cross-diffusion coefficients for a loaded AOT microemulsion, a quaternary system containing water (1)/AOT (2)/species (3)/octane (4). Here "species" is a component of the Belousov−Zhabotinsky reaction: NaBr, $NaBrO_3$, bathoferroin, ferroin, or Br_2. The main and cross-diffusion coefficients of each species depend crucially on its solubility. For water-soluble species (the salts), D_{13} and D_{23} are large (much larger than the main diffusion coefficients) and positive. For species located mainly in the surfactant shell (bathoferroin or ferroin), D_{13} and D_{23} are large and negative. For oil-soluble Br_2, D_{13} and D_{23} are larger and more negative, whereas $D_{33} \gg D_{11}, D_{22}$. The coefficients D_{31} and D_{32} are small for all species studied.

1. Introduction

The primary mechanisms of pattern formation in reaction−diffusion systems include excitability for traveling trigger waves (e.g., spirals or concentric rings),[1,2] bistability for labyrinthine or localized patterns,[3] Turing instability for temporally stationary, spatially periodic patterns,[4−6] and wave instability (sometimes called the finite wavenumber Hopf instability) for standing waves.[4,7] In all cases, the reacting species are assumed to obey simple Fickian diffusion, where "simple" in this context means that the diffusivity matrix, **D**, is diagonal. The ratios between the diagonal elements of **D**, the main diffusion coefficients, are critical in determining the mechanism of pattern formation. For example, for Turing instability, $D_{\text{inhibitor}}$ must be significantly larger than $D_{\text{activator}}$, where $D_{\text{activator}}$ and $D_{\text{inhibitor}}$ are the diffusion coefficients, respectively, of a species that grows autocatalytically and of one that inhibits the autocatalysis.

A more general treatment of reaction−diffusion systems allows for the possibility of cross-diffusion, in which a flux of one species can be induced by a gradient of another species. Cross-diffusion, if it occurs, can affect all of the above mechanisms of pattern formation[8] and may play a significant role in many patterns previously described. Examples include patterns in a CFUR (continuously fed unstirred reactor), where the gradients of species across a feeding gel layer may be large,[9,10] and the Belousov−Zhabotinsky (BZ) reaction dispersed in water-in-oil aerosol OT (AOT) microemulsion, (BZ-AOT system),[11−13] where large cross-diffusion effects (for example, a flux of water molecules induced by a flux of AOT molecules) are well documented.[14−16] For this reason, more detailed information about the effects of cross-diffusion in pattern-forming reaction−diffusion systems is essential for understanding the mechanism of pattern formation. In this article, we continue our investigation of cross-diffusion in the BZ-AOT system.

In a previous article,[17] we extended the Taylor dispersion method[18,19] to enable measurement of cross-diffusion in four-component systems because four is the minimum number of species for a loaded water-in-oil AOT microemulsion. Although the Taylor method is not as precise as Rayleigh interferometry on a Gosting diffusiometer,[20,21] information on cross-diffusion coefficients obtained by the Taylor method is sufficient to evaluate the importance (or lack of importance) of cross-diffusion for pattern formation. In the systems of interest here, species 1 is water, 2 is AOT, 3 is a component of the BZ reaction, and 4 is oil (octane in our case). Using this improved Taylor method, we examined two BZ species, malonic acid (MA) and ferroin, and found that the off-diagonal elements of the Fickian diffusivity matrix **D**, D_{13} and D_{23}, are large and positive ($D_{13}/D_{33} \cong 14$, $D_{23}/D_{33} \cong 3$) for MA and large and negative for ferroin ($D_{13}/D_{33} \cong -112$, $D_{23}/D_{33} \cong -30$), whereas the coefficients D_{31} and D_{32} are small and negative for MA ($D_{31}/D_{33} \cong -0.01$, $D_{32}/D_{33} \cong -0.14$) and small and positive for ferroin ($D_{31}/D_{33} \cong 5 \times 10^{-4}$, $D_{32}/D_{33} \cong 8 \times 10^{-3}$).[17] A positive (negative) cross-diffusion coefficient, D_{ij}, implies that species i diffuses toward smaller (larger) concentrations of species j. To complete the first stage of our investigation, we now determine cross-diffusion coefficients for the remaining species in the BZ reaction.

Here we present results on the main and cross-diffusion coefficients for four additional BZ species with quite different hydrophilic−hydrophobic properties. We investigate sodium bromate, which is the oxidizing agent in the BZ reaction; sodium bromide, which acts as an inhibitor and is a key species in the oscillatory behavior; a metal complex, such as bathoferroin (BF), which catalyzes the reaction; and finally, molecular bromine, which is a BZ-inhibiting intermediate formed during the reaction between bromate and bromide in acidic solution. The four species partition quite differently in the microemulsion (ME): bromate and bromide, as water-soluble salts, are located primarily in the water core of the nanodroplets. Because of the hydrophobic nature of the bathophenantroline ligand and the metal ion at its center, BF is soluble in neither water nor oil and should reside in the surfactant layer; this fact is reflected in a larger droplet radius measured in dynamic light scattering (DLS) experiments. Finally, the partition coefficients of Br_2 between octane (oil) and water (W) ($[Br_2]_{oil}/[Br_2]_W \cong 20$)[22] and

* Corresponding author.
[†] Brandeis University.
[‡] University of Siena.

10.1021/jp102753b
Published on Web 05/28/2010

between AOT and octane ($[Br_2]_{AOT}/[Br_2]_{oil} \cong 5$)[23] indicate that this species is preferentially located in the oil phase (because the volume of octane is much greater than that of AOT) at the small droplet fraction, φ_d, used in our experiments.

To establish the dependence of the main and cross-diffusion coefficients on the concentration of droplets, we also measure the diffusion matrix **D** for one of the BZ components, namely, ferroin, at several volume fractions and a constant droplet radius.

In Section 2, we present elements of the theory of the Taylor dispersion method used in our determinations. In Section 3 we explain our experimental methods. Our results appear in Section 4, and we conclude with a discussion in Section 5. Some cumbersome but useful equations are grouped in the Appendix.

2. Data Analysis: Theory

In quaternary systems (three solutes + solvent), the diffusion matrix **D** contains nine elements, namely, the three diagonal main diffusion coefficients, D_{ii}, and the six off-diagonal cross diffusion coefficients D_{ij}, $i,j = 1, 2, 3$ ($i \neq j$). As the solvent in our water-in-oil microemulsion, we choose the continuous phase, the oil (component 4). In our recent article,[17] we extended the Taylor dispersion technique, which involves the diffusive spreading of a drop of solution injected into a laminarly flowing stream containing the same components at slightly different concentrations, by developing two methods to calculate the nine diffusion coefficients in a four-component system. In the first approach, we employ only a refractive index detector (RID) to record the eluted Taylor peaks and make the assumption that the addition of the fourth (BZ) component to the three-component (ME) system does not significantly affect the interactions between the original three components. For example, we assume that the addition of bromate (component 3) to a pure AOT ME leaves the coefficients D_{11}, D_{12}, D_{21}, and D_{22} essentially unchanged. For relatively low concentrations of this added component, this is likely to be a reasonably accurate approximation. However, further fitting of the Taylor peaks by a set of Gaussian curves can improve the final result, especially at higher concentrations of the BZ component. Our second method requires the use of an additional detector, for example, a spectrophotometer, to measure the concentration of at least one component (note that the RID records the total signal from all components), for example Br_2 or BF.

In both methods, we first calculate the coefficients, F_{ij}, of a matrix **F** that links the partial derivatives of the concentrations, c_i, of all components in the flowing stream

$$\frac{\partial c_i}{\partial t} = \sum_{j=1}^{3} F_{ij} \frac{\partial^2 c_j}{\partial z^2} \tag{1}$$

where the concentration c_i of the ith component is related to its volume fraction φ_i as

$$\varphi_i = c_i M_i / d_i \tag{2}$$

where M_i is its molecular weight and d_i is its density. The coefficients F_{ij} have the same dimensions as the diffusion coefficients D_{ij} (cm^2/s), but they are inversely proportional to D_{ij}.[17−19] The F_{ij} can be obtained from the experimentally found parameters $P_{i,exp}$, K_i, and σ_i through the following equations

$$l_0^{-1} \sum_{i=1}^{n} P_{i,exp} = \sum_{i=1}^{n} K_i c_{i0} \tag{3}$$

$$l_0^{-1} \sum_{i=1}^{n} \sigma_i P_{i,exp} = \sum_{j=1}^{n} c_{j0} \sum_{i=1}^{n} K_i F_{ij} \tag{4}$$

where l_0 is the length of the capillary occupied by the sample injected at the initial time ($l_0^{-1} = \pi R_0^2/V_0$, V_0 is the injected volume, R_0 is the inner radius of the tubing), $P_{i,exp}$ are the pre-exponential parts of the Gaussian functions used to fit the experimental peaks, σ_i are the dispersions of the Gaussian functions, which are equal to the eigenvalues of the dispersion matrix **F**, c_{i0} is the difference between the concentration of component i in the injected sample and in the carrier stream, and K_i is the instrumental sensitivity with respect to that component (typically linear in the concentration). The experimentally measurable quantities $P_{i,exp}$, K_i, and σ_i can be found by fitting all experimental peaks $v(t)$ (generated with injections of different compositions) according to

$$v(t) = \sum_{i=1}^{3} \frac{P_{i,exp}}{\sqrt{4\pi\sigma_i t}} \exp\left[-\frac{u_0^2 (t - t_0)^2}{4\sigma_i t}\right] \tag{5}$$

where u_0 is the mean velocity of the carrier stream and t_0 is the retention time. Roughly speaking, t_0 corresponds to the maximum or minimum of the Taylor peak. Before applying eq 5, we calculate and subtract a baseline of the form ($a + bt$) from the measured signal.

The coefficients K_i can be found by analyzing three experiments involving injections with only $c_{10} \neq 0$, $c_{20} \neq 0$, or $c_{30} \neq 0$ as

$$K_i = l_0^{-1} \left(\sum_{j=1}^{3} P_{j,exp\_i} \right) / c_{i0} \quad i = 1, 2, 3 \tag{6}$$

and P_{j,exp_i} is the amplitude obtained for the jth Gaussian by fitting the experiment in which only $c_{i0} \neq 0$.

Finally, the diffusion coefficients D_{ij} can be derived from the coefficients F_{ij} through the relation[17]

$$D_{ij} = \frac{R_0^2 u_0^2}{48 \det(\mathbf{F})} \det(\mathbf{M}_{Fji})(-1)^{(i+j)} \tag{7}$$

where $\det(\mathbf{M}_{Fji})$ is the determinant of the minor associated with element F_{ji} of matrix **F**.

3. Experimental Section

Experiments were performed with a high-pressure liquid chromatography apparatus adapted with a long Teflon capillary in the place of the chromatography column to match the Taylor dispersion conditions.[18,24] The capillary was coiled in a 50 cm diameter helix, and its length was ~30 m between the injector and the spectrophotometer cell (Shimadzu UV-1650PC) and 32 m between the injector and the cell of the differential flow-through RID (Agilent 1100 series). The inner radius R_0 (= 0.42 mm) of the tubing was determined by gravimetry. An isocratic pump (Agilent G1310A), which maintained a steady flow, was placed between the eluent reservoir and the injector (Reodine).

A sample loop of volume 20 μL (= V_0) was used for injections. In addition to the Taylor peaks recorded by RID, signals were detected spectrophotometrically at $\lambda = 532$ nm in experiments with bathoferroin (molar extinction coefficient, $\varepsilon_{532} = 19\,270$ M^{-1} cm^{-1}) and at $\lambda = 400$ nm with bromine ($\varepsilon_{400} = 172$ M^{-1} cm^{-1}). The HPLC flow-thru cell (Shimadzu) had a 1 mm inner diameter and path length $l_c = 1$ cm (8 μL inner volume). Both detectors were connected to a personal computer for data acquisition.

The injector and capillary Teflon tubing were kept at 23 °C in a thermostatted incubator (Fisher Scientific). The flow rate was 0.15 mL/min for all experiments.

We also used a DLS apparatus (DynaPro, Protein Solutions, High Wycombe, U.K.) to monitor the size of water droplets in the AOT microemulsion loaded with a reactant of the BZ reaction. The mean radius of a droplet water core in a pure AOT microemulsion is roughly given by $R_w/\text{nm} = 0.17\omega$,[25−27] where $\omega = [H_2O]/[AOT]$; R_w is independent of the octane volume fraction in the microemulsion. We use $\omega = 11.84$ in our experiments. The total radius of the droplet plus the surrounding AOT monolayer (hydrodynamic radius), R_d, exceeds R_w by the length of an AOT molecule (∼1.1 nm), and the DLS method allows us to measure R_d.

Many physical properties of microemulsions show a threshold-like dependence on φ_d, the volume fraction of the dispersed phase ($\varphi_d = \varphi_{H_2O} + \varphi_{AOT}$). This dependence is due to percolation.[28−30] If $\varphi_d \ll \varphi_{cr}$ (the percolation threshold, $\varphi_{cr} \approx$ 0.5 to 0.6), then the microemulsion can be accurately characterized as a medium in which water droplets float freely. We worked at $\varphi_d = 0.18$, except in the case of ferroin, where we explored a range of $\varphi_d < \varphi_{cr}$.

Water-in-oil microemulsions were prepared using bidistilled water, AOT (sodium bis(2-ethylhexyl)sulfosuccinate, Aerosol OT, Aldrich) and octane (Sigma, analytical grade). Octane was further purified by mixing with concentrated H_2SO_4 for 2 days; a stock solution of AOT in octane ([AOT] = 1.5 M) was prepared and filtered through a 0.45 μm Teflon filter to remove possible impurities.

Sodium bromate, $NaBrO_3$ (SIGMA), sodium bromide, NaBr (Fisher), ferroin (Fluka), and molecular bromine, Br_2 (SIGMA), were used as received. We prepared bathoferroin by dissolving the desired amount of bathophenanthroline (4,7-diphenyl-1,10-phenanthroline, Aldrich) in a 1.5 M solution of AOT in octane and then adding a 0.25 M $FeSO_4$ aqueous solution in the ratio $[BP]/[Fe^{2+}] = 3$. In the following, we specify concentrations of H_2O, AOT, $NaBrO_3$, NaBr, ferroin, Br_2, BF, and octane with respect to the total volume of the microemulsion. Samples were injected every 3 h.

Using the Taylor dispersion method for a three-component system, we first measured the diffusion coefficients of the ternary AOT system (pure AOT microemulsion)[17] at the chosen ω (= 11.84) and φ_d (= 0.18). We obtained $D_{11} = 0.6 \pm 0.04 \times 10^{-6}$ cm^2/s, $D_{12} = 7.8 \pm 2 \times 10^{-6}$ cm^2/s, $D_{21} = -0.01 \pm 0.002 \times 10^{-6}$ cm^2/s, and $D_{22} = 1.3 \pm 0.04 \times 10^{-6}$ cm^2/s. Data for other values of φ_d will be presented in Section 4.

For each BZ component, we followed the same experimental and analytical procedures. Several samples with an excess or a defect of one or more of the three solutes were injected into the flowing solution. The experimental dispersion peaks obtained for each system were simultaneously fitted using eq 5 with $i =$ 1, 2, 3 to extract experimental parameters $P_{i,exp}$ and σ_i. (In all of our systems, the indices 1, 2, and 3 correspond to H_2O, AOT, and the BZ component, respectively.) The experimental parameters together with the diffusion coefficients D_{ij} ($i,j = 1, 2$) were used to calculate the dispersion coefficients F_{ij} according to eqs A1−A9 in the Appendix.

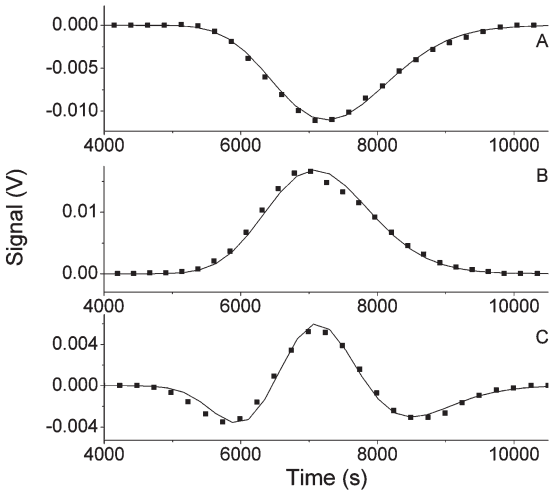

Figure 1. Taylor dispersion peaks for the four-component system water/AOT/$NaBrO_3$/octane. Squares are experimental data points and solid curves show analytical signals built using values from Table 1. Injected samples contain (A) an excess of H_2O, $\Delta[H_2O] = 1.5$ M, $\Delta[AOT] = \Delta[NaBrO_3] = 0$, (B) an excess of AOT, $\Delta[AOT] = 0.1$ M, $\Delta[H_2O] = \Delta[NaBrO_3] = 0$, and (C) an excess of $NaBrO_3$, $\Delta[NaBrO_3] = 0.04$ M, $\Delta[H_2O] = \Delta[AOT] = 0$. Composition of the carrier stream (eluent) is $[H_2O] = 3.552$ M, [AOT] = 0.3 M, $[NaBrO_3] = 1.6 \times 10^{-4}$ M, [octane] = 5.046 M ($\omega = 11.84$, $\varphi_d = 0.18$), $T = 23$ °C.

TABLE 1: Quaternary Diffusion Coefficients (in cm^2/s) for the Water (1)/AOT (2)/$NaBrO_3$ (3)/Octane System at $\omega = 11.84$, $\varphi_d = 0.18$, $[NaBrO_3] = 1.6 \times 10^{-4}$ M, and $T = 23$ °C

j	D_{j1}	D_{j2}	D_{j3}
1	$(6.4 \pm 0.5) \times 10^{-7}$	$(7.1 \pm 3) \times 10^{-6}$	$(8.1 \pm 1) \times 10^{-6}$
2	$(-1.1 \pm 0.2) \times 10^{-8}$	$(1.5 \pm 0.3) \times 10^{-6}$	$(1.9 \pm 0.06) \times 10^{-6}$
3	$(-3.1 \pm 7) \times 10^{-9}$	$(-7.3 \pm 2) \times 10^{-8}$	$(4.3 \pm 0.6) \times 10^{-7}$

The values of D_{ij} calculated from eq 7 were successively refined to get the best match between the experimental and analytical peaks, with the constraint that the eigenvalues of matrix **D** must be real and positive.

4. Results

4.1. $NaBrO_3$ and NaBr. The squares in Figure 1 represent the RID experimental signals obtained by injecting an excess of H_2O (panel A), an excess of AOT (panel B), and an excess of bromate (panel C) into the carrier stream. The fitting procedure yielded sensitivity coefficients $K_1 = -2$ V/M, $K_2 =$ 42 V/M, and $K_3 = -8$ V/M. The K_i can be either positive or negative because they represent differences among the sensitivities of the instrument with respect to the solute and the solvent. The values for K_1 and K_2 are consistent with results obtained for the ternary system, supporting our assumption that the ME structure is not changed significantly by the addition of bromate. The solid lines in Figure 1 represent the fitted curves obtained with the aid of eq 5. The diffusion coefficients deduced from these curves are reported in Table 1. The complex shape of the peak in Figure 1C demonstrates the presence of coupled flows, that is, fluxes of H_2O or AOT induced by the gradient of $NaBrO_3$. In the absence of cross-diffusion, these peaks would be simple Gaussians.

If we use NaBr as the fourth component, instead of $NaBrO_3$, the recorded Taylor dispersion peaks have almost the same shape as those in Figure 1. The diffusion coefficients calculated for the water/AOT/NaBr/octane system with $K_1 = -2.06$ V/M, K_2

TABLE 2: Quaternary Diffusion Coefficients (in cm²/s) for the Water (1)/AOT (2)/ NaBr (3)/Octane System at ω = 11.84, φ_d = 0.18, [NaBr] = 0.01 M, and T = 23 °C

j	D_{j1}	D_{j2}	D_{j3}
1	$(6.3 \pm 0.3) \times 10^{-7}$	$(6.3 \pm 2) \times 10^{-6}$	$(8 \pm 1) \times 10^{-5}$
2	$(-1 \pm 0.3) \times 10^{-8}$	$(1.2 \pm 0.2) \times 10^{-6}$	$(4.7 \pm 0.8) \times 10^{-6}$
3	$(2.3 \pm 3) \times 10^{-9}$	$(-3.7 \pm 2) \times 10^{-8}$	$(4.7 \pm 1) \times 10^{-7}$

= 52.6 V/M, and $K_3 = -30$ V/M are reported in Table 2. We see that for both $NaBrO_3$ and NaBr, the coefficients D_{31} and D_{32} are very small, whereas D_{13} and D_{23} are large and positive.

4.2. Bathoferroin. In experiments with the BZ catalyst BF, we experience the same problem we encountered with ferroin,[17] namely, that the DLS measurements indicate a bimodal distribution (Figure 2) of droplet radii at the rather large concentration of BF used in the injected sample. The peak at high R_h suggests the presence of clusters with a radius of 9 nm. Clearly, the formation of clusters shows that the added component (BF) affects the ME significantly; consequently, the diffusion coefficients D_{11}, D_{12}, D_{21}, and D_{22} found for the pure microemulsion will almost surely be different for a microemulsion loaded with BF. Second, clusters may have their own (smaller) diffusion coefficients and may require additional equations and experiments. Fortunately, in the case of BF, we can employ a spectrophotometer as a second detector for that species. Because none of the other species present in solution absorbs in the visible range, it is feasible to detect a single Gaussian dispersion profile for BF; consequently, we can calculate σ_3 with high precision. Moreover, we can also estimate F_{33} without using data from the three-component system (pure microemulsion) because we have $K_1 = K_2 = 0$, and if only $c_{30} \neq 0$, eq 4 gives $F_{33} = \sigma_3 P_{3,exp}/(c_{30} l_0 K_3)$.

Figure 3 shows the experimental dispersion curves for three injections with compositions different from the carrier solution. Panels A−C present the RID signal, whereas panel D shows the spectrophotometric signal recorded at λ = 532 nm for the experiment shown in panel C. Note that the concentration of BF at the maximum of the Taylor peak in Figure 3D ($\cong$ 6.42 × 10^{-5} M + 0.1/19000 M $\cong$ 6.9 × 10^{-5} M) is significantly smaller than that in the injected sample. At such small concentrations of BF, the DLS spectrum has a dominant maximum at R_h = 2 nm. Therefore, the concentration of clusters decreases over the course of our experiment, which suggests that the coefficients in the diffusivity matrix found below should be interpreted with some caution. From the fitting of the experimental Taylor peaks (solid curves in Figure 3), we calculated the RID sensitivity coefficients ($K_1 = -2.4$ V/M, K_2 = 43.2 V/M, and K_3 = 600 V/M) and the diffusion coefficients reported in Table 3. Note that coefficient D_{12} is almost two times smaller than in the pure microemulsion or the microemulsion loaded with $NaBrO_3$. Presumably, this change results from the effect of BF on the structure of the microemulsion (clustering).

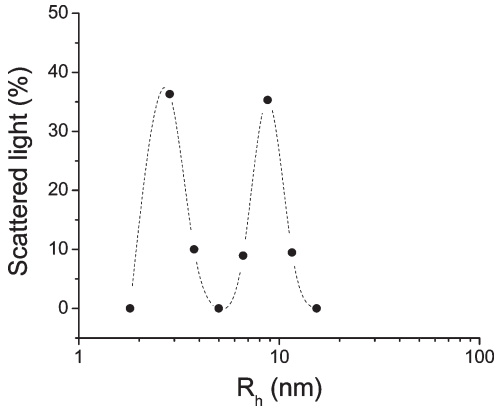

Figure 2. Dependence of the intensity of scattered light upon the hydrodynamic radius of the droplets in a microemulsion with ω = 11.84, φ_d = 0.18, and [BF] = 2 × 10^{-3} M. $T \cong$ 24 °C.

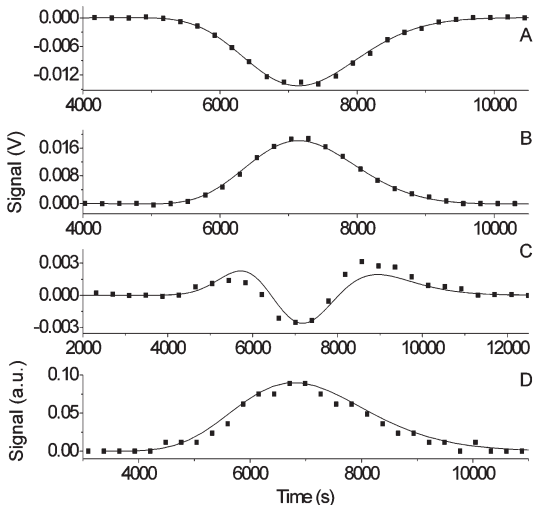

Figure 3. Taylor dispersion peaks for the four-component system water/AOT/BF/octane. (A−C) Signals of RID and (D) spectrophotometric absorption at λ = 532 nm. Squares show experimental data and solid curves show analytical signals built using values from Table 3. Injected samples contain (A) an excess of H_2O, $\Delta[H_2O]$ = 1.5 M, Δ[AOT] = Δ[BF] = 0, (B) an excess of AOT, Δ[AOT] = 0.1 M, $\Delta[H_2O]$ = Δ[BF] = 0, and (C,D) an excess of BF, Δ[BF] = 1.5 × 10^{-3} M, $\Delta[H_2O]$ = Δ[AOT] = 0. Composition of the carrier stream (eluent) is $[H_2O]$ = 3.552 M, [AOT] = 0.3 M, [BF] = 6.42 × 10^{-5} M, [octane] = 5.046 M (ω = 11.84, φ_d = 0.18), T = 23 °C.

TABLE 3: Quaternary Diffusion Coefficients (in cm²/s) for the Water (1)/AOT (2)/BF (3)/Octane System at ω = 11.84, φ_d = 0.18, [BF] = 6.42 × 10^{-5} M, and T = 23 °C

j	D_{j1}	D_{j2}	D_{j3}
1	$(6.2 \pm 0.4) \times 10^{-7}$	$(3.5 \pm 1) \times 10^{-6}$	$(-7.3 \pm 1) \times 10^{-5}$
2	$(-1 \pm 0.2) \times 10^{-8}$	$(1.2 \pm 0.2) \times 10^{-6}$	$(-2 \pm 0.1) \times 10^{-5}$
3	$(3.4 \pm 6) \times 10^{-12}$	$(4.8 \pm 1) \times 10^{-9}$	$(1.9 \pm 0.3) \times 10^{-7}$

4.3. Br_2. In the case of Br_2 as the fourth component, it is also possible to use a spectrophotometer as a second detector. The availability of a second detector is quite important here because the volatile nature of Br_2 makes the measurement of its diffusivity more challenging if we use only RID. Molecular bromine can escape from the Teflon tubing, as can be seen from the slope of the time series shown in Figure 4, where the absorbance of bromine was recorded at λ = 400 nm.

Figure 5 shows the Taylor peaks for three different injections into the flowing solution (with excesses of (A) H_2O, (B) AOT, and (C) Br_2). The calculated diffusivities are reported in Table 4, where we see that the main diffusion coefficient for Br_2, D_{33}, is two orders of magnitude larger than that for $NaBrO_3$ and BF. As expected from its solubility properties, the main diffusion coefficient of bromine is of the same order of magnitude as that of octane (2.63 × 10^{-5} cm²/s).

4.4. Cross-Diffusion at Different φ_d. The matrix **D** of diffusion coefficients in the water/AOT/ferroin/octane system calculated at three different droplet fractions φ_d (= 0.1, 0.18, and 0.25) and constant ω (= 11.84) is reported in Table 5 and Figure 6. The main diffusion coefficients D_{11} and D_{22} (the ternary subsystem) as well as D_{33} are found to decrease at higher values of φ_d in parallel with the viscosity of the solution. These

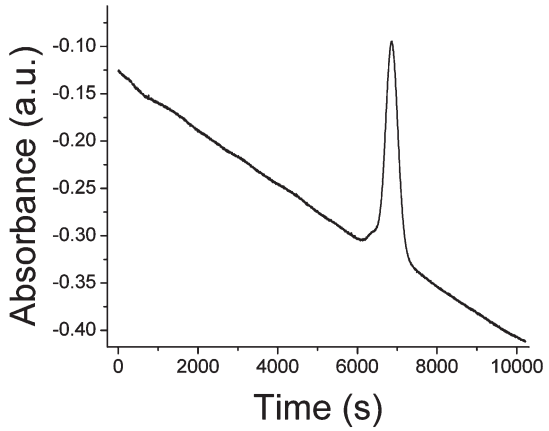

Figure 4. Spectrophotometric time series of Br_2 absorbance at λ = 400 nm. The time series and experimental conditions correspond to the RID signal in Figure 5C.

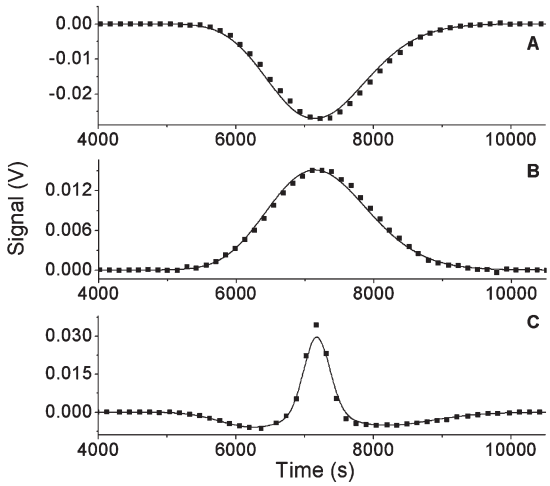

Figure 5. Taylor dispersion peaks for the four-component system water/AOT/Br_2/octane. Squares are experimental data and solid curves show analytical signals built using values from Table 4. Injected samples contain (A) an excess of H_2O, $\Delta[H_2O] = 1.5$ M, $\Delta[AOT] = \Delta[Br_2] = 0$, (B) an excess of AOT, $\Delta[AOT] = 0.1$ M, $\Delta[H_2O] = \Delta[Br_2] = 0$, and (C) an excess of Br_2, $\Delta[Br_2] = 0.1$ M, $\Delta[H_2O] = \Delta[AOT] = 0$. Composition of the carrier stream (eluent) is $[H_2O] = 3.552$ M, [AOT] = 0.3 M, $[Br_2] = 5 \times 10^{-3}$ M, [octane] = 5.046 M ($\omega = 11.84$, $\varphi_d = 0.18$), $T = 23$ °C.

TABLE 4: Quaternary Diffusion Coefficients (in cm^2/s) for the Water (1)/AOT (2)/Br_2 (3)/Octane System at $\omega = 11.84$, $\varphi_d = 0.18$, $[Br_2] = 5 \times 10^{-3}$ M, and $T = 23$ °C

j	D_{j1}	D_{j2}	D_{j3}
1	$(6.3 \pm 0.4) \times 10^{-7}$	$(6.6 \pm 3) \times 10^{-6}$	$(-1.3 \pm 0.2) \times 10^{-4}$
2	$(-1 \pm 0.2) \times 10^{-8}$	$(1.2 \pm 0.2) \times 10^{-6}$	$(-2.6 \pm 0.09) \times 10^{-6}$
3	$(0.6 \pm 1.5) \times 10^{-7}$	$(-9.8 \pm 3) \times 10^{-7}$	$(1.9 \pm 0.3) \times 10^{-5}$

findings are in line with previously reported results for the ternary system.[14,31] The counter-flows of water and AOT induced by ferroin (proportional to coefficients D_{13} and D_{23}, respectively), decrease significantly with droplet fraction, whereas the values of D_{31} and D_{32} remain almost constant.

Using DLS to monitor the changes in the ME structure, we have found, as expected, that the presence of clusters (Figure 2) diminishes when the concentration of droplets is decreased, whereas the droplets' hydrodynamic radius (R_h) increases slightly. This dependence of R_h on φ_d can be explained by the fact that the ratio [ferroin]/[droplets] approaches unity as φ_d decreases, and, as a result, the molecular volume of the catalyst contributes significantly to the average size and the shape of the droplets. The reduction in magnitude of the coefficients D_{13} and D_{23} with increasing φ_d can be explained in part by the smaller effect of [ferroin] on the structure of the nanodroplets at larger φ_d and in part by the smaller interaction between ferroin and AOT as well as between ferroin and water in the droplet clusters.

5. Discussion

The Taylor peaks reported in Figures 1 and 3−5 show that samples containing an excess of injected water or AOT generate curves with similar shapes for all systems analyzed. In contrast, samples containing an excess of one of the BZ reagents give a distinctive profile for each of the four species, $NaBrO_3$, NaBr, BF, and Br_2. The peaks for $NaBrO_3$ (Figure 1C) and NaBr resemble the previously obtained peaks for MA and sodium malonate under analogous conditions.[17] The Taylor peaks for BF (Figure 3C) and for ferroin[17] also resemble one another. Generalizing these data, we suggest that the peak shapes and consequently the sign and magnitude of the diffusion coefficients in the four-component system, water/AOT/species/octane, are largely determined by the solubility properties of the BZ species.

For water-soluble species like $NaBrO_3$, NaBr, MA, and sodium malonate,[17] the species resides primarily in the water cores of the nanodroplets. The diffusion coefficient of the BZ reactant, D_{33}, is therefore of the same order of magnitude as that of H_2O (D_{11}). The cross-diffusion coefficients D_{13} and D_{23}, which account for the coupled flows of the BZ reactant induced, respectively, by water and AOT, are large and positive, whereas the cross-diffusion coefficients, D_{31} and D_{32}, which account for the flows induced by the BZ reactant in water and AOT, are small.

In the case of BF, as well as ferroin, where most of the species can be found in the surfactant shell of the nanodroplet, the main diffusion coefficient, D_{33}, is also of the same order of magnitude as D_{11} (for H_2O), but the cross-diffusion coefficients show a very different behavior: large and negative D_{13} and D_{23} and small and positive D_{31} and D_{32}.

The oil-soluble Br_2 gives a peak with a positive sharp central maximum and two broad negative tails. As previously noted, the main diffusion coefficient, D_{33}, for this species, is two orders of magnitude larger than that of bromate and BF. It is also interesting to note that the signs of the (rather small) cross-diffusion coefficients D_{31} and D_{32} are opposite, in contrast with the results obtained for the other BZ species. Finally, D_{13} and D_{23} were found to be large and negative, as in the case of BF.

We attempt here to provide some insight into the above behavior. A key result is that[31]

$$D_{ii} = D_i^* + C_i(\partial D_i^*/\partial C_i) \quad (8)$$

$$D_{ik} = C_i(\partial D_i^*/\partial C_k), (i \neq k) \quad (9)$$

where D_i^* is the solute intradiffusion or self-diffusion coefficient of species i and C_i is the concentration of that species. Leaist[31] has discussed the behavior of the three-component (water−AOT−oil) system, in particular, the coefficients D_{11}, D_{12}, D_{21}, and D_{22}. Increasing the concentration of water in the microemulsion at constant [AOT] leads to a larger average droplet size and a lower mobility of the droplets so that the partial derivative term in eq 8 is negative for $i = 1$. Increasing C_2, that is, [AOT], gives smaller, more mobile droplets and a positive value of $\partial D_2^*/\partial C_2$. The self-diffusion coefficients, D_1^* and D_2^*, are roughly equal to the diffusion coefficient of the drops. This

TABLE 5: Diffusion Coefficients, D_{ij} (in cm^2/s), and Sensitivity Coefficients, K_i, for the Water (1)/AOT (2)/Ferroin (3)/Octane System at Several φ_d with $\omega = 11.84$ and $T = 23$ °C

[ferroin] (M)	3.57×10^{-5}	1.61×10^{-5}	2.58×10^{-5}
φ_d	0.1	0.18	0.25
D_{11}	$(1.2 \pm 0.07) \times 10^{-6}$	$(5.0 \pm 0.3) \times 10^{-7}$	$(3 \pm 0.2) \times 10^{-7}$
D_{12}	$(1.7 \pm 0.7) \times 10^{-6}$	$(5.2 \pm 2) \times 10^{-6}$	$(4.5 \pm 2) \times 10^{-6}$
D_{13}	$(-1.2 \pm 0.2) \times 10^{-4}$	$(-4.5 \pm 0.6) \times 10^{-5}$	$(-4.7 \pm 0.7) \times 10^{-6}$
D_{21}	$(-1.6 \pm 0.3) \times 10^{-9}$	$(-1.2 \pm 0.2) \times 10^{-8}$	$(-9.8 \pm 2) \times 10^{-9}$
D_{22}	$(1.6 \pm 0.3) \times 10^{-6}$	$(1.2 \pm 0.2) \times 10^{-6}$	$(9.6 \pm 2) \times 10^{-7}$
D_{23}	$(-2.8 \pm 0.09) \times 10^{-5}$	$(-1.2 \pm 0.04) \times 10^{-5}$	$(-6.4 \pm 0.2) \times 10^{-6}$
D_{31}	$(-0.64 \pm 2) \times 10^{-9}$	$(2.2 \pm 5) \times 10^{-10}$	$(-1.1 \pm 3) \times 10^{-10}$
D_{32}	$(2.5 \pm 0.6) \times 10^{-9}$	$(3.2 \pm 0.8) \times 10^{-9}$	$(8.3 \pm 2) \times 10^{-9}$
D_{33}	$(1 \pm 0.1) \times 10^{-6}$	$(4 \pm 0.6) \times 10^{-7}$	$(1.3 \pm 0.2) \times 10^{-7}$
K_1 (V/M)	−1.95	−2.05	−3.07
K_2 (V/M)	48	42.3	46
K_3 (V/M)	300	554	400

means that $\partial D_1^*/\partial C_2$ is positive and $\partial D_2^*/\partial C_1$ is negative. Therefore, the signs of $\partial D_i^*/\partial C_i$ and eqs 8 and 9 predict that $D_{11} < D_{22}$, D_{12} is positive, and D_{21} is negative, as observed.

For BF and Br_2, the formation of aggregates appears to play a major role in determining the cross-diffusion coefficients. In the case of BF, the tendency to form clusters of droplets noted above implies that increasing [BF] lowers the mobility of the species that travel with the droplets so that $\partial D_i^*/\partial C_3 < 0$ for both water ($i = 1$) and AOT ($i = 2$). Negative $\partial D_i^*/\partial C_3$ ($i = 1,2$) gives, according to eq 9, negative D_{i3} and, according to eq 8, D_{33} is smaller than D_{11} and D_{22}, as we observe. For bromine, although much of it resides in the oil (which leads to the large value of D_{33}), there is evidence of the formation of a 1:1 AOT-Br_2 complex,[23] which would increase the bulk of a droplet in a region of high [Br_2], lowering its mobility in much the same way as BF-mediated cluster formation. Therefore, we also expect $\partial D_i^*/\partial C_3 < 0$ when species 3 is bromine.

For the water-soluble BZ components, we expect $D_{33} \approx D_{11}$ because that species is essentially confined to the aqueous phase. As suggested in our previous work,[17] the most plausible mechanism appears to be "excluded volume" for water-soluble BZ components. The larger concentration of NaBr or $NaBrO_3$ induces a larger effective concentration of water in the droplet because the volume available for motion of water in the aqueous pseudophase becomes smaller. In the "excluded volume" mechanism, the cross-diffusion coefficients can be expressed as

$$D_{ik} = D_{ii} V_k c_i / (1 - \varphi_k)^2 \tag{10}$$

where V_k is the molar volume and $\varphi_k = V_k c_k$ is the volume fraction of the salt in the aqueous phase.[32] The "excluded volume" hypothesis explains well the positive cross-diffusion coefficient D_{13}. The positive value found for D_{23}, that is, the tendency of AOT molecules to diffuse toward smaller concentrations of water-soluble BZ species, may result from a small decrease in the droplet radius with increasing salt concentration due to the electrical screening effect of the salt on the repulsion between the SO_3^- groups of the AOT. This screening can reduce the radius of the droplets, resulting in positive $\partial D_2^*/\partial C_3$ and consequently positive D_{23}.

In all of our systems, the coefficients D_{31} and D_{32} are comparable to our experimental error, that is, indistinguishable from zero in our experiments. We attribute their small magnitude to the fact that $C_3 \ll C_1$, C_2 and the proportionality of D_{3j} to C_j,

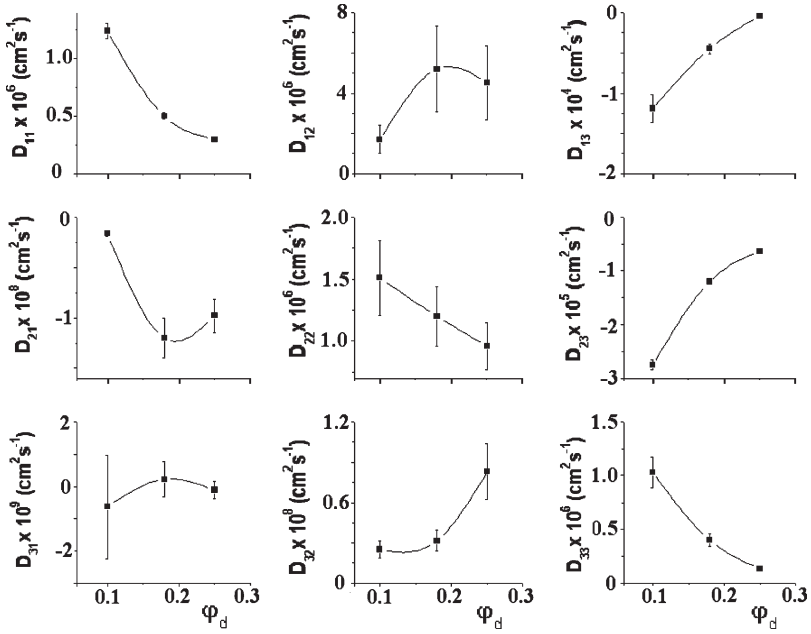

Figure 6. Dependence of the main- and cross-diffusion coefficients for the system water/AOT/ferroin/octane on the droplet fraction φ_d. $\omega = 11.84$, $T = 23$ °C.

because the partial derivative terms in eq 9 should be comparable to the derivatives with respect to the other species present in the drops.

To evaluate the significance of the cross-diffusion coefficients found in this work for pattern formation in the BZ-AOT system, we also require the cross-diffusion coefficients between species involved in the BZ reaction, that is, cross-diffusion coefficients in five-component systems (AOT microemulsions loaded with two BZ species). We intend to attack this challenging problem in future work, in which the data obtained here for four-component systems will play a vital role.

Acknowledgment. This work was supported in part by the National Science Foundation through grant CHE-0526866. F.R. was supported by a Marie Curie International Outgoing Fellowship within the 7th European Community Framework Programme.

Appendix

We give here the equations used to calculate the quantities F_{ij} from the experimentally measured quantities.

$$F_{11} = (D_{22}\sigma_1\sigma_2\sigma_3/K_{FD} + F_{13}F_{31})/F_{33} \quad \text{(A1)}$$

$$F_{12} = (W_2 - K_2F_{22} - K_3F_{32})/K_1 \quad \text{(A2)}$$

$$F_{13} = [F_{33}K_2(\sigma_1 + \sigma_2 + \sigma_3 - F_{33}) - K_2(1/s_1 + 1/s_2)\sigma_1\sigma_2\sigma_3 + (K_3F_{33} - W_3)F_{32}]/(K_2F_{31} - K_1F_{32}) \quad \text{(A3)}$$

$$F_{21} = (W_1 - K_1F_{11} - K_3F_{31})/K_2 \quad \text{(A4)}$$

$$F_{22} = \sigma_1 + \sigma_2 + \sigma_3 - F_{11} - F_{33} \quad \text{(A5)}$$

$$F_{23} = [F_{33}K_1(\sigma_1 + \sigma_2 + \sigma_3 - F_{33}) - K_1(1/s_1 + 1/s_2)\sigma_1\sigma_2\sigma_3 + (K_3F_{33} - W_3)F_{31}]/(K_1F_{32} - K_2F_{31}) \quad \text{(A6)}$$

$$F_{31} = (K_{FD}W_1F_{33} + K_2D_{21}\sigma_1\sigma_2\sigma_3 - K_1D_{22}\sigma_1\sigma_2\sigma_3)/(K_{FD}W_3) \quad \text{(A7)}$$

$$F_{32} = (K_{FD}W_2F_{33} + K_1D_{12}\sigma_1\sigma_2\sigma_3 - K_2D_{11}\sigma_1\sigma_2\sigma_3)/(K_{FD}W_3) \quad \text{(A8)}$$

$$F_{33} = \sigma_1\sigma_2\sigma_3/s_1s_2 \quad \text{(A9)}$$

where s_1 and s_2 are the dispersion of the Gaussian functions for the three-component system, $W_i = l_0^{-1}(\sum_{j=1}^{3}\sigma_jP_{j,\exp\_i})/c_{i0}$, and $K_{FD} \equiv R_0^2u_0^2/48$.

References and Notes

(1) Zaikin, A. N.; Zhabotinsky, A. M. *Nature* **1970**, *225*, 535.

(2) Winfree, A. T. *Science* **1972**, *175*, 634–636.

(3) Vanag, V. K.; Epstein, I. R. *Chaos* **2007**, *17*, 037110.

(4) Turing, A. M. *Philos. Trans. R. Soc., B* **1952**, *237*, 37–72.

(5) Vanag, V. K.; Epstein, I. R. *Phys. Rev. Lett.* **2001**, *87*, 228301.

(6) Castets, V.; Dulos, E.; Boissonade, J.; De Kepper, P. *Phys. Rev. Lett.* **1990**, *64*, 2953–2956.

(7) Vanag, V. K. R.; Epstein, I. *Phys. Rev. Lett.* **2002**, *88*, 088303.

(8) Vanag, V. K.; Epstein, I. R. *Phys. Chem. Chem. Phys.* **2009**, *11*, 897–912.

(9) Horváth, J.; Szalai, I.; De Kepper, P. *Science* **2009**, *324*, 772−775.

(10) Ouyang, Q.; Swinney, H. L. *Nature* **1991**, *352*, 610–612.

(11) Epstein, I. R.; Vanag, V. K. *Chaos* **2005**, *15*, 047510.

(12) Vanag, V. K. *Phys.-Usp.* **2004**, *47*, 923–941.

(13) Vanag, V. K. Epstein, I. R. Chapter 5. In *Patterns of Nanodroplets: The Belousov-Zhabotinsky-Aerosol OT-Microemulsion System*; Springer: Berlin, 2008; Vol. 99, pp 89−113.

(14) Leaist, D. G.; Hao, L. *J. Phys. Chem.* **1995**, *99*, 12896–12901.

(15) Costantino, L.; Dellavolpe, C.; Ortona, O.; Vitagliano, V. *J. Chem. Soc., Faraday Trans.* **1992**, *88*, 61–63.

(16) Costantino, L.; Dellavolpe, C.; Ortona, O.; Vitagliano, V. *J. Colloid Interface Sci.* **1992**, *148*, 72–79.

(17) Vanag, V. K.; Rossi, F.; Cherkashin, A. A.; R Epstein, I. *J. Phys. Chem. B* **2008**, *112*, 9058–9070.

(18) Price, W. E. *J. Chem. Soc., Faraday Trans. 1* **1988**, *84*, 2431–2439.

(19) Taylor, G. I. *Proc. Roy. Soc. A* **1953**, *219*, 186–203.

(20) Annunziata, O.; Vergara, A.; Paduano, L.; Sartorio, R.; Miller, D. G.; Albright, J. G. *J. Phys. Chem. B* **2003**, *107*, 6590–6597.

(21) Annunziata, O.; Vergara, A.; Paduano, L.; Sartorio, R.; Miller, D. G.; Albright, J. G. *J. Phys. Chem. B* **2009**, *113*, 13446–13453.

(22) Toiya, M.; Vanag, V. K.; Epstein, I. R. *Angew. Chem., Int. Ed.* **2008**, *47*, 7753–7755.

(23) Garcia-Rio, L.; Mejuto, J. C.; Ciri, R.; Blagoeva, I. B.; Leis, J. R.; Ruasse, M.-F. *J. Phys. Chem. B* **1999**, *103*, 4997–5004.

(24) Alizadeh, A.; DeCastrro, C. A. N.; Wakeham, W. A. *Int. J. Thermophys.* **1980**, *1*, 243–284.

(25) Fletcher, P. D. I.; Howe, A. M.; Robinson, B. H. *J. Chem. Soc., Faraday Trans.* **1987**, *83*, 985–1006.

(26) Kotlarchyk, M.; Chen, S. H.; Huang, J. S. *J. Phys. Chem.* **1982**, *86*, 3273–3276.

(27) Ray, S.; Bisal, S. R.; Moulik, S. P. *J. Chem. Soc., Faraday Trans.* **1993**, *89*, 3277–3282.

(28) van Dijk, M. A.; Casteleijn, G.; Joosten, J. G. H.; Levine, Y. K. *J. Chem. Phys.* **1986**, *85*, 626–631.

(29) Chen, S. H.; Ku, C. Y.; Rouch, J.; Tartaglia, P.; Cametti, C.; Samseth, J. *J. Phys. IV* **1993**, *3*, 143–161.

(30) Peyrelasse, J.; Mohaouchane, M.; Boned, C. *Phys. Rev. A* **1988**, *38*, 4155–4161.

(31) Leaist, D. G. *Phys. Chem. Chem. Phys.* **2002**, *4*, 4732–4739.

JP102753B